Contributions to the cross shock electric field at a quasiperpendicular collisionless shock

J. P. Eastwood,[1] S. D. Bale,[1,2] F. S. Mozer,[1] and A. J. Hull[1]

Received 15 May 2007; revised 19 July 2007; accepted 8 August 2007; published 13 September 2007.

[1] The normal electric field structure of a supercritical (M_{ms} = 5.2), quasiperpendicular (θ_{Bn} = 70°) collisionless shock is examined using Cluster four-spacecraft observations of the terrestrial bow shock. Comparing the observed electric field with magnetic field and plasma observations, two different techniques find that the $\mathbf{J} \times \mathbf{B}/ne$ term in the generalized Ohm's law accounts for a majority of the large-scale normal electric field and potential drop encountered by the ions - the solar wind ion deceleration is in good empirical agreement with the observed potential drop, confirming earlier work. Large amplitude electric field fluctuations on shorter timescales, corresponding to fine scale structure, are not observed to contribute to the ion energization. **Citation:** Eastwood, J. P., S. D. Bale, F. S. Mozer, and A. J. Hull (2007), Contributions to the cross shock electric field at a quasiperpendicular collisionless shock, *Geophys. Res. Lett.*, *34*, L17104, doi:10.1029/2007GL030610.

1. Introduction

[2] The terrestrial bow shock is the most studied example of a collisionless shock in space. Investigations have mainly concentrated on the quasiperpendicular shock, particularly its magnetic structure and the behavior of different particle species as they traverse the shock [*Tsurutani and Stone*, 1985; *Bale et al.*, 2005]. However very few studies of electric field structure have been published, despite the fact that the electric field is of central importance to the deceleration process. Furthermore, shocks are important sites for particle acceleration in a number of astrophysical and heliophysical contexts with the electric field again playing a key role [*Lee et al.*, 1996; *Kucharek et al.*, 2004]. In-situ observations of the electric field at Earth's bow shock provide important and unique experimental data that can be used to understand the details of plasma thermalization and energetic particle production in more general circumstances as a function of both plasma beta and Mach number.

[3] The first observations of the normal electric field at Earth's bow shock were based on ISEE-1 data [*Heppner et al.*, 1978; *Formisano*, 1982]; examples of both supercritical [*Scudder et al.*, 1986a] and subcritical [*Wygant et al.*, 1987] shocks have been published. More recent studies with Cluster [*Walker et al.*, 2004] and Polar [*Bale and Mozer*, 2007] have concentrated on the small-scale (c/ω_{pe}) structure of the field within the ramp. It is the purpose of this paper to investigate the electric field in more detail, and in particular, to specifically examine the terms in the generalized Ohm's law (equation (1)) [*Rossi and Olbert*, 1970] that support the shock electric field. The terms on the right hand side of equation (1) are referred to as the dispersive, ambipolar, viscous, resistive and inertial terms respectively.

$$\mathbf{E} + \mathbf{v} \times \mathbf{B} \approx \frac{\mathbf{J} \times \mathbf{B}}{ne} - \frac{\nabla \cdot P_e}{ne} - \frac{M_e}{M_i}\frac{\nabla \cdot P_i}{ne} + \eta \mathbf{J} + \frac{M_e}{ne^2}\frac{d\mathbf{J}}{dt} \quad (1)$$

[4] A terrestrial bow shock encounter made by the Cluster spacecraft on 7 April 2002, when the shock was supercritical, is examined. The four-spacecraft nature of the data [*Escoubet et al.*, 2001] allows theories of the shock structure to be tested more stringently, and with new techniques. For example, multi-spacecraft data can be used to determine the orientation and motion of boundaries [*Schwartz*, 1998] and to estimate the current density within the tetrahedron [*Dunlop et al.*, 2002]. Here we use these techniques to study the structure of the cross-shock electric field, and to determine the contribution of the $\mathbf{J} \times \mathbf{B}$/ne term in the generalized Ohm's law to the normal electric field.

2. Observations

[5] Cluster encountered the bow shock at ~01:27UT, at [13, −6, 7] Re (Geocentric Solar Ecliptic coordinates), during the outbound portion of the orbit on the dusk flank of the shock above the ecliptic plane. At this time, the tetrahedron scale size was ~100 km, comparable to the expected shock thickness [*Newbury et al.*, 1998; *Bale et al.*, 2003]. Observations of the magnetic field (at $22.42s^{-1}$) from the FGM experiment [*Balogh et al.*, 2001] together with ion plasma observations (at $0.25s^{-1}$) from the CIS experiment [*Rème et al.*, 2001] are shown in Figure 1. A 15 minute interval centered on the shock crossing is shown. The spacecraft pass from the downstream to the upstream side of the shock. Table 1 summarizes the up and downstream parameters measured by Cluster 3.

[6] Various techniques were used to determine the shock normal. Minimum Variance Analysis (MVA) [*Sonnerup and Scheible*, 1998] applied to the Cluster 3 spin ($0.25\ s^{-1}$) resolution magnetic field data in the interval 01:26UT–01:28UT resulted in a minimum variance direction of $\mathbf{n}$ = [0.953, −0.218, 0.211]. The ratio of intermediate to minimum eigenvalues is 10.8; the existence of a non-coplanar magnetic field component within the shock ramp (discussed below) ensured a good separation of the eigenvalues. Maximum variance analysis of the electric field resulted in a normal vector within ~8° of this estimate. A multi-spacecraft timing analysis applied to the magnetic field

[1]Space Sciences Laboratory, University of California, Berkeley, California, USA.
[2]Physics Department, University of California, Berkeley, California, USA.

0094-8276/07/2007GL030610$05.00

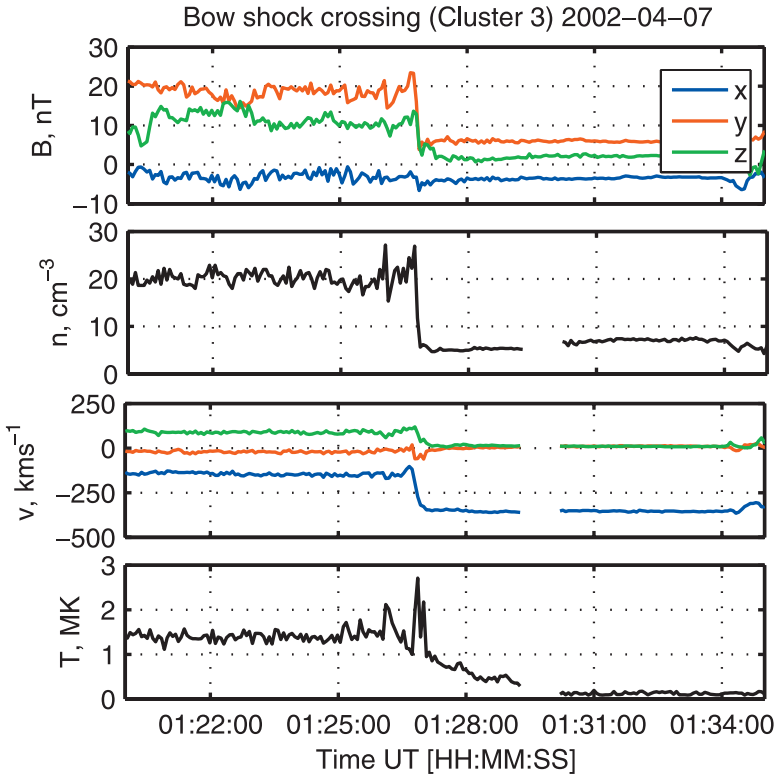

Figure 1. Cluster 3 observations of the Earth's bow shock at 01:27UT on 7 April 2002. Data from the FGM and CIS experiments are shown. Cluster moves from the downstream to the upstream side of the shock. The gap in the plasma data is due to an instrument change from magnetosheath to solar wind mode. Blue, red and green correspond to x, y and z GSE.

found the shock normal to be [0.9063, −0.0547, 0.4190] GSE, and a shock speed of −12 kms^{-1} [*Schwartz*, 1998]. The duration of the ramp crossing is ∼13 s thus indicating a shock thickness of ∼150 km. The angle between this normal and the MVA estimate is ∼15°. Since $\nabla \cdot \mathbf{B} = 0$, it is expected that $\mathbf{B} \cdot \mathbf{n}$ is constant across the shock. The MVA normal best satisfied this criterion.

[7] Using the average up and downstream magnetic field listed in Table 1 and the MVA normal, we find that θ_{Bn}, the angle between the shock normal and the magnetic field, is 70° in the upstream region and 88° in the downstream region. The ion inertial length c/ω_{pi} is ∼50 km in the magnetosheath, and ∼90 km in the solar wind. The convected ion gyroradius is ∼125 km [*Bale et al.*, 2005]. The upstream magnetosonic speed along $\mathbf{n}$ is ∼67 kms^{-1}, corresponding to a magnetosonic Mach number of 5.2. The upstream ion plasma $\beta = 0.6$; this shock is stronger and lower β than the example studied by *Scudder et al.* [1986b].

[8] The electric field is measured by the EFW experiment (at 25 s^{-1}) [*Gustafsson et al.*, 2001]. EFW uses 4 sensors at the end of wire booms to measure the components of the d.c. electric field in the spacecraft spin plane (∼ the GSE x-y plane). The third component of the electric field (along the spin axis) can be reconstructed using $\mathbf{B}$ (assuming that $\mathbf{E} \cdot \mathbf{B} = 0$), provided $\mathbf{B}$ is not too weak and does not lie in the spin plane. In this example, $\mathbf{B}$ was too close to the spin plane in the upstream solar wind to reconstruct E_z. However, the convection electric field could be calculated from the ion plasma moments and the magnetic field according to $\mathbf{E} = -\mathbf{v_i} \times \mathbf{B}$.

3. Cross-Shock Electric Field

[9] The data in Figure 1 are presented in the spacecraft frame and the GSE coordinate system. Since $\mathbf{E}$ is frame dependent, it is necessary to choose an appropriate frame in which to analyze the data [*Goodrich and Scudder*, 1984]. Two frames are of particular relevance; the Normal Incidence Frame (NIF) and the DeHoffmann-Teller Frame (HTF) [*De Hoffmann and Teller*, 1950]. In the NIF, the upstream flow is along the shock normal and $(\mathbf{v} \times \mathbf{B})_x = 0$. The HTF is typically more appropriate for the study of electron dynamics. The NIF is appropriate for the study of ion dynamics, and is the frame used in this paper. The data

Table 1. Average Plasma Properties in the Vicinity of the Bow Shock (Cluster 3)[a]

	Upstream	Downstream
Interval	01:31UT–01:33UT	01:24UT–01:26UT
$\|B\|$ (nT)	7.1	21.7
$\mathbf{B}$ (nT)	(−3.3, 5.8, 2.2)	(−2.8, 18.6, 10.7)
n (cm^{-3})	7.1	19.9
$\|v\|$ (kms^{-1})	354	173
$\mathbf{v}$ (kms^{-1})	(−354, 10, 9)	(−148, −21, 86)
T (MK)	0.129	1.42

[a]The upstream interval was observed after the downstream interval.

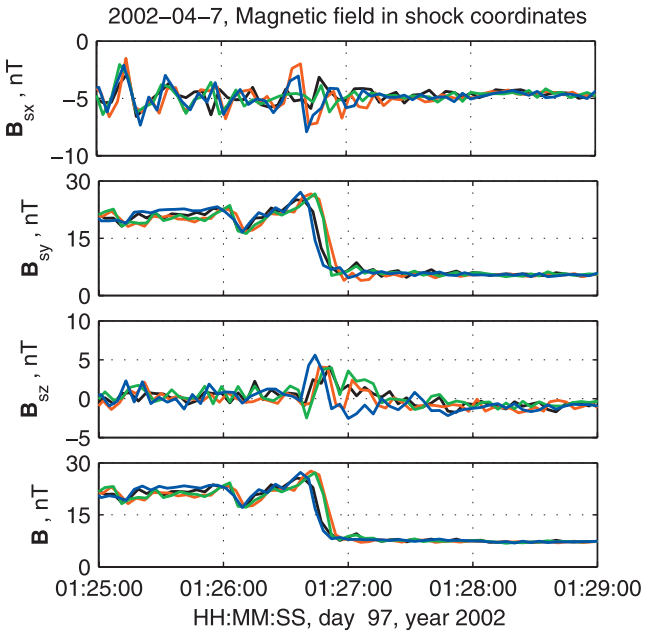

Figure 2. Magnetic field from the four Cluster spacecraft in shock coordinates. The upstream magnetic field points into the shock. The magnetic field is amplified mainly in the y direction, perpendicular to the shock normal. The z component is zero either side of the shock, but there is a positive deviation in B_z inside the shock ramp. This is consistent with the existence of a positive normal electric field, as discussed in the text. Different colors indicate the different spacecraft.

were also rotated into a boundary normal coordinate system such that the shock normal points along the x direction, the x-y plane defines the magnetic coplanarity plane based on the maximum and minimum magnetic variance direction calculated previously, and the z direction completes the right handed triple. Figure 2 shows the magnetic field in the shock coordinate system. As expected for a fast mode shock, there is a positive deviation in B_z inside the shock ramp [*Goodrich and Scudder*, 1984; *Thomsen et al.*, 1987; *Wygant et al.*, 1987].

[10] Figure 3 shows the NIF normal electric field measured by Cluster 3 (black line). Rather than simply identifying E_{xGSE} as the normal electric field [*Scudder et al.*, 1986b], the data were reconstructed before being transformed. The shock is quasiperpendicular, and so the normal electric field is nearly perpendicular to the magnetic field. The blue and red lines show two different calculations of $\mathbf{J} \times \mathbf{B}$/ne. For the first estimate (red line), the curlometer technique [*Dunlop et al.*, 2002] was applied to the interval 01:26UT–01:28UT. This technique linearly interpolates the magnetic field over the spacecraft tetrahedron to determine the curl of the magnetic field, and thus the current density from Ampere's law. It requires that the spacecraft are co-located in the shock ramp, which is the case for this event. Using density measurements from the EFW instrument (the spacecraft potential is a strong function of density [*Pedersen et al.*, 2001], and is measured at a higher time resolution ($5\ s^{-1}$) than particle instruments), $(\mathbf{J} \times \mathbf{B}/\mathrm{ne})_x$ can then be calculated; this estimate is shown as a red line in Figure 3. Note that the resolution of this estimate is limited to the time cadence of the density measurements. An alternative procedure (blue line), rather than using particle moments to compute $\mathbf{J}$ [*Scudder et al.*, 1986b], is to assume the shock is 1 dimensional and stationary, and differentiate $\mathbf{B}$ across the shock. This follows a similar procedure used to analyze Cluster observations of the Hall fields at a reconnection site on the magnetopause [*Vaivads et al.*, 2004]. Here, we can make use of the Cluster timing analysis; the speed of the shock allows the time series to be converted into a length scale. Having estimated $J_y(x)$ and $J_z(x)$, we can then compute $(\mathbf{J} \times \mathbf{B}/\mathrm{ne})_x = (J_y B_z - J_z B_y)/ne$ (in fact, $|J_z B_y| > |J_y B_z|$). This estimate is shown as the blue line in Figure 3, again at $5s^{-1}$ resolution. The two estimates of the Hall electric field agree reasonably well in magnitude and profile and it can be seen that the majority of the observed macro (i.e. ion)-scale electric field in the Normal Incidence frame is due to $\mathbf{J} \times \mathbf{B}$/ne.

[11] The normal field peaks at a few mVm^{-1}. This is consistent with the observed out-of-plane magnetic field. To first order, one can argue that $\mathbf{E} \cdot \mathbf{B} = E_x B_x + E_z B_z = 0$, where E_x is the normal electric field, B_x is the normal component of the magnetic field, E_z is the constant solar wind convection electric field, and B_z is the out-of-plane magnetic field in the shock ramp (in the NIF, $E_y = 0$). The convection electric field $\mathrm{E}_z \sim 2\ \mathrm{mVm}^{-1}$ (estimated from the ion data), $\mathrm{B}_x \sim -5$nT, and B_z peaks at ~5 nT, implying that E_x should be positive and peak at a few mVm^{-1}. The electrons remain essentially frozen to the magnetic field through the shock transition [*Scudder*, 1995]. They $\mathbf{E} \times \mathbf{B}$ drift out of the coplanarity plane in the shock ramp, which results in the out-of-plane magnetic field, analogous to the Hall magnetic fields observed in magnetic reconnection. The current that arises from the differential motion of the

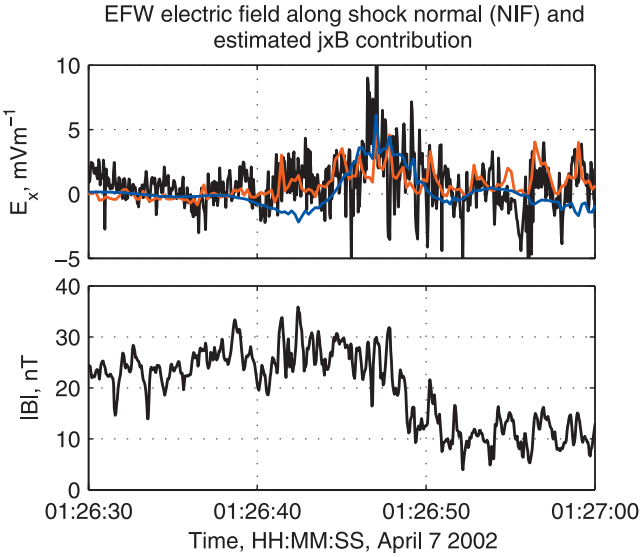

Figure 3. Comparison between the measured electric field in the Normal Incidence Frame (black), and the $\mathbf{J} \times \mathbf{B}$/ne electric field at Cluster 3 estimated using the curlometer technique (red) and via integration of the single-spacecraft data (blue).

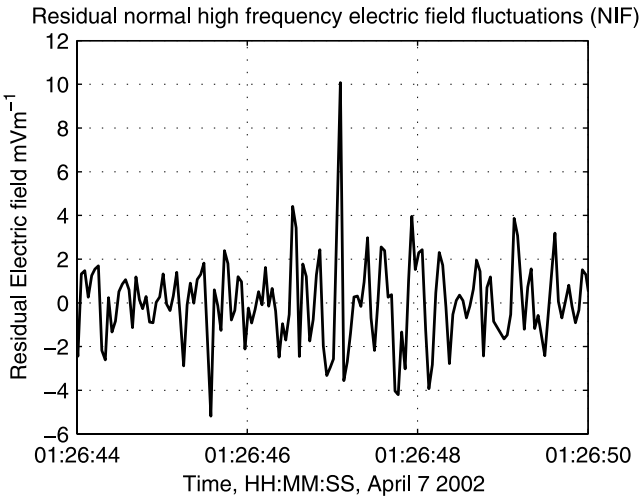

Figure 4. Residual high frequency fluctuations of the normal electric field in the NIF. The interval shown concentrates on the shock ramp.

ions and electrons self-consistently sustains the NIF electric field.

[12] We consider the consistency of the ion motion and the electric field. Between 01:26:32UT–01:26:52UT, the change in ion bulk velocity corresponds to an energy loss of ~260 eV. Integrating the normal electric field over the corresponding interval gives a potential drop of 266 V, in good agreement. Note that we have treated the data differently by integrating E_x rather than using a model profile [*Scudder et al.*, 1986a, 1986b].The integrated $\mathbf{J} \times \mathbf{B}$/ne contribution to the cross shock potential difference is found to be 165 V; this implies that the majority (~60–70%) of the normal electric field is due to the Hall term. Unfortunately, the shock crossing occurred too quickly for good measurements of the electron pressure gradient to be made. However, by using two independent techniques, the estimate of $\mathbf{J} \times \mathbf{B}$/ne is substantiated.

[13] Finally, we note that the integration of the electric field is insensitive to fluctuations at frequencies above 2.5 Hz. This is shown in Figure 4. Plotted is the electric field at full (25 Hz) resolution, with the linearly interpolated 5 Hz resolution data (used for comparison with the $\mathbf{J} \times \mathbf{B}$/ne calculations) subtracted. The potential drop associated with these fluctuations over the same interval as the previous calculations is 2 V. Although these fluctuations are large, with amplitudes that exceed the 'background' macro/ion-scale electric field structure, they do not contribute to the overall potential 'hill' encountered by the ions. The timescale for these fluctuations ranges from 2.5–12.5 Hz (the upper resolvable limit). While it is not the intent of this paper to characterize the nature of this fine structure, analysis shows no strong polarization of the wave activity, although we are limited by the time resolution of the data; candidates include whistlers, or ion acoustic waves downshifted into the observed frequency range. Studies of electrostatic ion acoustic waves at higher frequencies show a similar non-contribution to the overall potential drop [*Hull et al.*, 2006]. Nevertheless, these structures may still play a role in the thermalization of the plasma population via particle scattering.

4. Conclusions

[14] We have presented new observations of the electric field structure at Earth's quasiperpendicular bow shock. In this encounter, the shock normal electric field, presented on sub-second timescales in the NIF exhibited a large scale variation on the convecting ion inertial length scale, a significant component of which is due to the dispersive term in the generalized Ohm's law. A new method, the curlometer, was used to compute **J** and compared well with an second independent method based on integration of **B**. At a weaker shock, *Scudder et al.* [1986b] found that the ponderomotive force accounted for approximately half of the potential, and so further investigation is required to understand how different terms scale experimentally. This electric field is the main agent responsible for decelerating the ions; by directly integrating the electric field data, a good comparison was found between the potential change and the bulk ion deceleration. As such, it is also responsible for reflecting a portion of the inflowing ion distribution back into the upstream region leading to formation of the foreshock. Superposed on this large scale variation is much finer scale electric field structure, which although large in amplitude does not appear to contribute to the overall cross-shock potential. It is therefore likely that it does not influence the overall ion deceleration in this example but it may influence shock structure via thermalization.

[15] **Acknowledgments.** This work was supported by NASA grant NNG05GL27G at UC Berkeley. G. Paschmann is thanked for his comments and a number of useful discussions.

References

Bale, S. D., and F. S. Mozer (2007), Large parallel and perpendicular electric fields on electron spatial scales in the terrestrial bow shock, *Phys. Res. Lett.*, *98*, 205001.

Bale, S. D., F. S. Mozer, and T. S. Horbury (2003), Density-transition scale at quasiperpendicular collisionless shocks, *Phys. Res. Lett.*, *91*, 265004.

Bale, S. D., et al. (2005), Quasi-perpendicular shock structure and processes, *Space Sci. Rev.*, *118*, 161–203.

Balogh, A., et al. (2001), The cluster magnetic field investigation: Overview of inflight performance and initial results, *Ann. Geophys.*, *19*, 1207–1217.

De Hoffmann, F., and E. Teller (1950), Magneto-hydrodynamic shocks, *Phys. Rev.*, *80*(4), 692–703.

Dunlop, M. W., A. Balogh, K.-H. Glassmeier, and P. Robert (2002), Four-point Cluster application of magnetic field analysis tools: The curlometer, *J. Geophys. Res.*, *107*(A11), 1384, doi:10.1029/2001JA005088.

Escoubet, C. P., M. Fehringer, and M. L. Goldstein (2001), The Cluster mission, *Ann. Geophys.*, *19*, 1197–1200.

Formisano, V. (1982), Measurement of the potential drop across the Earth's collisionless bow shock, *Geophys. Res. Lett.*, *9*, 1033–1036.

Goodrich, C. C., and J. D. Scudder (1984), The adiabatic energy change of plasma electrons and the frame dependence of the cross-shock potential at collisionless magnetosonic shock waves, *J. Geophys. Res.*, *89*, 6654–6662.

Gustafsson, G., et al. (2001), First results of electric field and density observations by cluster efw based on initial months of operation, *Ann. Geophys.*, *19*, 1219–1240.

Heppner, J. P., N. C. Maynard, and T. L. Aggson (1978), Early results from ISEE-1 electric field measurements, *Space Sci. Rev.*, *22*, 777–789.

Hull, A. J., D. E. Larson, M. Wilber, J. D. Scudder, F. S. Mozer, and C. T. Russell (2006), Large-amplitude electrostatic waves associated with magnetic ramp substructure at Earth's bow shock, *Geophys. Res. Lett.*, *33*, L15104, doi:10.1029/2005GL025564.

Kucharek, H., E. M. Mobius, M. Scholer, C. Mouikis, L. M. Kistler, T. Horbury, A. Balogh, H. Reme, and J. M. Bosqued (2004), On the

origin of field-aligned beams at the quasi-perpendicular bow shock: multi-spacecraft observations by Cluster, *Ann. Geophys.*, *22*, 2301–2308.

Lee, M. A., V. D. Shapiro, and R. Z. Sagdeev (1996), Pickup ion energization by shock surfing, *J. Geophys. Res.*, *101*, 4777–4789.

Newbury, J. A., C. T. Russell, and M. Gedalin (1998), The ramp widths of high-Mach-number, quasi-perpendicular collisionless shocks, *J. Geophys. Res.*, *103*, 29,581–29,593.

Pedersen, A., et al. (2001), Four-point high time resolution information on electron densities by the electric field experiments (EFW) on Cluster, *Ann. Geophys.*, *19*, 1483–1489.

Rème, H., et al. (2001), First multispacecraft ion measurements in and near the Earth's magnetosphere with the identical Cluster Ion Spectrometry (CIS) experiment, *Ann. Geophys.*, *19*, 1303–1354.

Rossi, B., and S. Olbert (1970), *Introduction to the Physics of Space*, McGraw-Hill, New York.

Schwartz, S. J. (1998), Shock and Discontinuity Normals, Mach Numbers and Related Parameters, in *Analysis methods for multi-spacecraft data*, edited by G. Paschmann and P. W. Daly, pp. 249–270, Int. Space Sci. Inst., Bern.

Scudder, J. D. (1995), A review of the physics of electron heating at collisionless shocks, *Adv. Space Res.*, *15*(8/9), 181–223.

Scudder, J. D., A. Mangeney, C. Lacombe, C. C. Harvey, T. L. Aggson, R. R. Anderson, J. T. Gosling, G. Paschmann, and C. T. Russell (1986a), The resolved layer of a collisionless, high beta, supercritical, quasi-perpendicular shock wave: 1. Rankine-Hugoniot geometry, currents, and stationarity, *J. Geophys. Res.*, *91*, 11,019–11,052.

Scudder, J. D., A. Mangeney, C. Lacombe, C. C. Harvey, and T. L. Aggson (1986b), The resolved layer of a collisionless, high beta, supercritical, quasi-perpendicular shock wave: 2. Dissipative fluid electrodynamics, *J. Geophys. Res.*, *91*, 11,053–11,073.

Sonnerup, B. U. O., and M. Schieble (1998), Minimum and Maximum Variance Analysis, in *Analysis methods for multi-spacecraft data*, edited by G. Paschmann and P. W. Daly, pp. 185–220, Int. Space Sci. Inst., Bern.

Thomsen, M. F., J. T. Gosling, S. J. Bame, K. B. Quest, D. Winske, W. A. Livesey, and C. T. Russell (1987), On the noncoplanarity of the magnetic field within a fast collisionless shock, *J. Geophys. Res.*, *92*, 2305–2314.

Tsurutani, B. T., and R. G. Stone (1985), *Collisionless Shocks in the Heliosphere: Reviews of Current Research*, *Geophys. Monogr. Ser.*, vol. 35, edited by B. T. Tsurutani and R. G. Stone, AGU, Washington D. C.

Vaivads, A., Y. Khotyaintsev, M. André, A. Retinò, S. Buchert, B. N. Rogers, P. Décréau, G. Paschmann, and T. D. Phan (2004), Structure of the magnetic reconnection diffusion region from four-spacecraft observations, *Phys. Res. Lett.*, *93*, 105001.

Walker, S. N., H. Alleyne, M. Balikhin, M. Andre, and T. S. Horbury (2004), Electric field scales at quasi-perpendicular shocks, *Ann. Geophys.*, *22*, 2291–2300.

Wygant, J. R., M. Bensadoun, and F. S. Mozer (1987), Electric field measurements at subcritical, oblique bow shock crossings, *J. Geophys. Res.*, *92*, 11,109–11,121.

S. D. Bale, J. P. Eastwood, A. J. Hull, and F. S. Mozer, Space Sciences Laboratory, 7 Gauss Way, University of California, Berkeley, CA 94720, USA. (eastwood@ssl.berkeley.edu)